Click Here for Full Article

Observations of infragravity waves at the ocean-bottom broadband seismic stations Endeavour (KEBB) and Explorer (KXBB)

David Dolenc

Seismological Laboratory, University of California, Berkeley, McCone Hall 215, Berkeley, California 94720, USA

Now at Large Lakes Observatory, University of Minnesota, 109 RLB, 2205 East 5th Street, Duluth, Minnesota 55812, USA (ddolenc@d.umn.edu)

Barbara Romanowicz

Seismological Laboratory, University of California, Berkeley, McCone Hall 215, Berkeley, California 94720, USA

Paul McGill

Monterey Bay Aquarium Research Institute, 7700 Sandholdt Road, Moss Landing, California 95039, USA

William Wilcock

School of Oceanography, University of Washington, Box 357940, Seattle, Washington 98195, USA

[1] We report observations of infragravity waves in the period band 30–400 s at two buried broadband ocean-bottom seismic stations, KEBB and KXBB, located off the coast of the Pacific Northwest, at a water depth of ∼2370 m. When compared to the energy of short-period ocean waves recorded at local buoys, the low-frequency seismic noise is found to be mainly generated when the short-period ocean waves reach the coast, and not when the storm passes directly above the station. Two types of modulation of the infragravity signal are observed. First, a longer-period modulation is observed and is best correlated with the energy of the 14–16 s period ocean waves. Second, the entire infragravity band signal is modulated in phase with tides. The results suggest that the infragravity waves originate from the nearshore region east of buoy 46041, which lies off the coast of Washington State, and not from the nearshore regions farther to the north that are closer to KEBB. Strong polarization of the KEBB horizontal motions in the NW–SE direction also suggests that the infragravity waves arrive at KEBB from the SE direction. Since the infragravity waves are not generated uniformly along the shore, modeling of their spatial variability prior to the selection of new sites could help improve the quality of future ocean-bottom seismic deployments and may also help understand processes at the origin of the Earth's low-frequency hum.

1. Introduction

[2] The primary reason for installing ocean-bottom broadband seismic stations is to record earthquakes. Observations of nonseismic signals, like infragravity waves, are often regarded as noise and additional processing is needed to remove them. At the same time, observations of infragravity waves at the ocean-bottom broadband stations can be used to study their generation and propagation.

[3] Infragravity waves are ocean surface waves with periods longer than wind-driven waves and swell. Their wave amplitudes in the deep water are small (<1 cm) and their wave band stretches from 20 s period to tidal periods [*Webb*, 1998]. Infragravity waves are generated by nonlinear interactions between short-period ocean waves (periods between 5 and 20 s) in the nearshore region [*Longuet-Higgins and Stewart*, 1962; *Herbers et al.*, 1995a]. Since the sloping continental shelf acts as a waveguide, the infragravity waves are typically about 40 dB more energetic over the shelf than in the deep ocean [*Webb*, 2007a]. Part of the infragravity energy leaks off the shelf and propagates into deep water [*Webb et al.*, 1991; *Okihiro et al.*, 1992]. At the ocean bottom these waves couple into seismic waves via pressure fluctuations. The transfer of energy into seismic waves occurs mainly over the shallow shelf where the infragravity waves are larger [*Webb*, 2007a]. Infragravity waves were first observed near the shore by *Munk* [1949] and *Tucker* [1950]. In oceanography, infragravity waves are important for nearshore processes such as sediment transport [*Holman and Bowen*, 1982], currents in the surf zone [*Kobayashi and Karjadi*, 1996], and oscillations in harbors [*Okihiro et al.*, 1993]. In seismology, seafloor deformation under the pressure forcing due to infragravity waves results in increased long-period noise at the ocean bottom that can be observed in the 20 to 500 s period band [*Webb et al.*, 1991; *Webb*, 1998].

[4] Ocean-bottom seismic stations are needed to study offshore faults and seismicity, to improve azimuthal coverage when studying tectonic processes at the continental edge, as well as to obtain more uniform global station coverage for the study of the Earth's interior. Carefully installed borehole installations a few hundred meters below the seafloor may be the best approach to provide good coupling with the ocean floor while avoiding the long-period noise due to infragravity waves, but they remain very expensive [*Stephen et al.*, 2003]. The results from deployments so far showed that more affordable shallow buried seismic installations also provide good coupling with the ocean floor sediments [e.g., *Stephen et al.*, 2003; *Duennebier and Sutton*, 2007], and that postprocessing can be used to remove part of the long-period seismic noise as well as signal-generated noise to significantly improve the quality of seismic observations [*Webb and Crawford*, 1999; *Crawford and Webb*, 2000; *Dolenc et al.*, 2007].

[5] Since the infragravity waves result in long-period seismic noise, they are often considered to be an unavoidable nuisance for seismic observations. However, the ever present long-period seismic noise can also be viewed as a passive source and used to determine the density and elastic parameters of the oceanic crust and upper mantle [e.g., *Crawford et al.*, 1991, 1998]. In addition, recent studies showed that continuously excited normal modes of the Earth are due to excitation sources that lie under the oceans [*Rhie and Romanowicz*, 2004; *Tanimoto*, 2005], and that Earth's "hum" is driven by infragravity waves over the continental shelves [*Rhie and Romanowicz*, 2006; *Webb*, 2007a]. *Webb* [2007b] further suggested that infragravity waves interacting over the deep ocean basins also contribute to the Earth's "hum." Understanding the nature and characteristics of the coupling between infragravity waves and the solid earth is therefore important not only for the studies of the generation and dissipation of infragravity waves, but also for the study of the Earth's "hum" and Earth structure using nonseismic sources.

2. Ocean-Bottom Broadband Seismic Stations Endeavour (KEBB) and Explorer (KXBB)

[6] Ocean-bottom broadband stations KEBB (47.96 N, 129.12 W) and KXBB (49.50 N, 129.00 W) were deployed as part of a 3-year
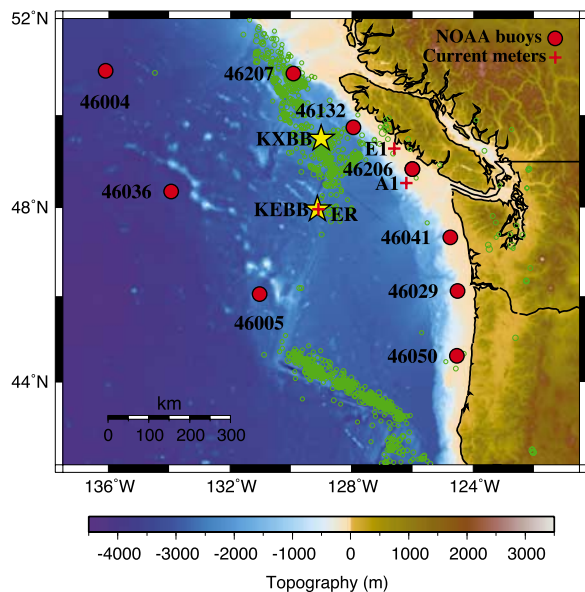
Figure 1. Bathymetric and topographic map showing the locations of seismic stations KEBB and KXBB (yellow stars), nearby NOAA and Canadian MEDS buoys (red filled circles), and ocean current meters (red pluses). Background seismicity (ANSS catalog, M4+, 1981–2006) is shown by green circles.

multidisciplinary experiment funded by the W. M. Keck foundation to monitor the linkages between seismic deformation and hydrothermal fluxes on the northern Juan de Fuca plate [*McGill et al.*, 2003, 2004; *Wilcock et al.*, 2007]. The seismic component of the project was a collaboration between the University of Washington, the University of Oregon, and the Monterey Bay Aquarium Research Institute. Station KEBB was installed 247 km offshore Vancouver Island on the Pacific Plate adjacent to the Endeavour Segment of the Juan de Fuca Ridge at a water depth of 2376 m in August 2003 (Figure 1). A year later station KXBB was installed 105 km offshore Vancouver Island on the Explorer Plate at a water depth of 2370 m. Each station comprised a three-component broadband Guralp CMG-1T seismometer, sensitive over a wide frequency range, from 50 Hz to 2.8 mHz (360 s), connected to a recording and battery package. Both seismometers were completely buried in the ocean floor sediments, recording continuous data at 50 Hz autonomously. The KEBB data were retrieved in August 2004 and September 2005, and the instrument recovered in August 2007. The KXBB data and instrument were retrieved in September 2005. The third ocean-bottom broadband seismic station (KNBB) was

also deployed in the region from August 2004 to September 2005, at the base of the continental slope offshore Nootka Sound, as part of the same project, but could not be included in the analysis as the recorded data included too many gaps [*Barclay*, 2005].

3. Power Spectral Density

[7] We first compared the power spectral density (PSD) at KEBB, MOBB and YBH (Figure 2) for the vertical and horizontal component. Station MOBB is a permanent broadband ocean-bottom seismic station located 40 km offshore Monterey Bay, California, at a water depth of 1000 m [*Romanowicz et al.*, 2006]. Land station YBH is one of the quietest Berkeley Digital Seismic Network (BDSN) stations, located 560 km north of MOBB, near Yreka, California. Results for a quiet day (left, 17 September 2003) and for a stormy day (right, 8 October 2003) are shown. Four hours of data (0000–0400 UTC) were used in the calculation. The quiet and the stormy day were selected on the basis of the spectral wave density (SWD) measured at the NOAA buoys 46041 (near KEBB) and 46042 (near MOBB). There were no significant earthquakes recorded during the two time periods.

[8] The KEBB and MOBB vertical component data show a noise "hump" for periods longer than 30 s and 20 s, respectively. The noise "hump" is due to deformation of the seafloor under the pressure forcing by the infragravity waves and is not observed at the land station YBH. Since only linear waves with wavelengths comparable or larger than the water depth can generate a detectable pressure signal at the seafloor [*Webb*, 1998], the additional water column at KEBB results in a higher value of the short-period cutoff of the noise "hump" at KEBB than at MOBB. The overall lower noise "hump" observed at KEBB than at MOBB for the vertical component is a result of the (1) additional water column at KEBB, (2) different seafloor compliance at KEBB and MOBB, and (3) different properties of the incoming ocean waves from which the infragravity waves were generated locally. The observed peak at KEBB and MOBB is stronger and wider (periods up to 400 s) on a stormy day. The narrow peaks observed at KEBB at 20 s and 30 s are probably due to instrumental noise and are present throughout the deployment. The noise at KEBB and MOBB between 10 and 20 s is comparable to the quietest
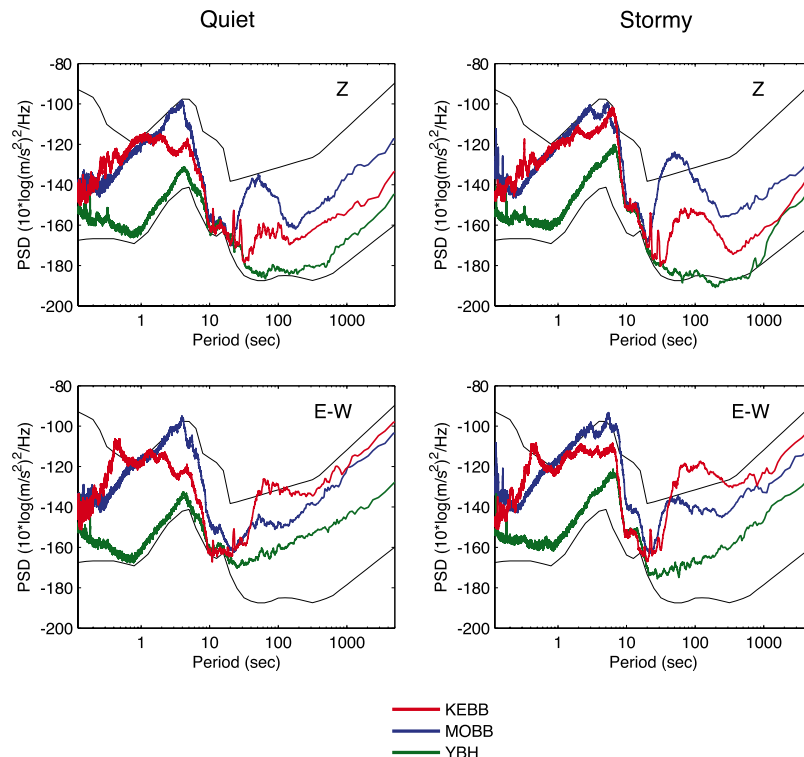
Figure 2. Power spectral density (PSD) at KEBB, MOBB, and YBH (560 km north of MOBB, one of the quietest BDSN stations) for the vertical (top) and horizontal (bottom) component. Results for a quiet (left, 17 September 2003) and for a stormy day (right, 8 October 2003) are shown. The USGS high- and low-noise models for land stations are shown in black.

BDSN land stations. The primary or single-frequency microseism peak at 14 s is observed at all three stations. Figure 2 also shows a strong secondary or double-frequency microseism peak with significantly higher microseismic noise levels observed at the two ocean-bottom stations than at the land station. Within the microseismic band, a hint of three peaks is observed between 1 and 10 s (best seen at MOBB E−W component on the stormy day). The three peaks are often observed at sites in the Pacific and are, in order of increasing period, a result of the local wind-wavefield, local storms in the North Pacific, and the large storms in the Southern Ocean [*Webb*, 1992, 1998]. It is not unusual, however, to observe only the two peaks that are due to the local wind-wavefield and storms in the distant Southern Ocean. Although microseisms mostly propagate as fundamental mode Rayleigh waves, some of the microseism peak structure also results from the shift from the fundamental to the higher-order Rayleigh waves. On the horizontal KEBB component a strong peak is also observed between 0.4 and 0.5 s. This peak is probably due to short-wavelength shear modes (Stoneley or Sholte waves) that are often seen in the horizontal spectra above 1 Hz [*Webb*, 1998].

[9] The results for the two horizontal components were similar and therefore only one component (E−W) is shown in Figure 2. In this case the long-period noise is stronger at KEBB than at MOBB. The infragravity "hump" on the KEBB horizontals is stronger than on the vertical component; this is not a surprise and similar observations have been made during previous ocean-bottom broadband deployments [*Stephen et al.*, 2003]. Stronger long-period noise on the horizontal components is also predicted theoretically [*Araki et al.*, 2004]. This is due to tilt, which, in addition to horizontal displacements, contributes significantly to the long-period noise on the horizontal components. Observations during the MOBB deployment [*Romanowicz et al.*, 2006] showed that it took MOBB about two months to settle in the sediments after the initial deployment, suggesting that it is important to re-level the seismometer a few months after the installation.

[10] The shape of the noise spectra in the infragravity wave band measured at KEBB agrees with observations from previous deployments in which seismometers were buried under the ocean floor [e.g., *Stephen et al.*, 2003; *Araki et al.*, 2004], as well as with theoretical predictions [*Crawford et al.*, 1998; *Araki et al.*, 2004]. The study by *Crawford et al.* [1998] showed that at seafloor depths of 2.2–2.7 km, the infragravity signals are expected to be observed between approximately 30 and 290 s and that in this range the contribution from the direct seafloor displacements due to deformation is dominant. The horizontal seismometer components are sensitive to tilts as well as to horizontal displacements.

[11] The second year of the KEBB deployment and the single year of the KXBB deployment were both significantly noisier than the first year of the KEBB deployment. They both showed increased overall noise as well as stronger instrumental noise. The number of data gaps also increased significantly [*Barclay*, 2005], which further limited the use of these data for infragravity wave studies. The work presented in this paper is therefore based primarily on the first year of data from station KEBB. An example of data from the noisy deployment period for which we also used an additional algorithm to remove the data gaps is shown in Appendix A (Figure A1).

4. Generation of Infragravity Signal

[12] We computed PSD spectrograms for 1-h long segments for all the available KEBB data and compared the results to the SWD measured at the nearby NOAA and Canadian MEDS buoys. The SWD is computed at the buoys once every hour and it measures energy of the ocean waves in m^2/Hz in the 0.01 Hz wide frequency bins between 0.03 and 0.4 Hz. Spectrograms for a 7-d period (13–20 February 2004) are presented in Figure 3. The infragravity peak can be observed in the PSD plot for the vertical KEBB channel throughout the 7-d period (Figure 3b, top panel). The signal observed on the vertical KEBB channel just below 30 s and at 20 s is probably due to instrumental noise and is present throughout the deployment, and the strong signal observed as a single vertical line at periods shorter than 50 s on day 2004.049 is due to an Mw 5.8 Gulf of California earthquake. The vertical black line indicates a sudden change of the infragravity peak width and amplitude. The second panel from the top shows the SWD measured at the westernmost buoy 46036, and the panel below at the southernmost deep water buoy 46005. The remaining 4 panels show the SWD at the nearshore buoys ordered by longitude. The mean wave direction corresponding to energy of the dominant period measured at buoy 46041 showed that the waves observed on day 2004.048 were approaching from the WSW direction, which was also the direction from which the storm was approaching. Increased energy of the 5–20 s ocean waves on day 2004.048 can therefore first be seen on buoys 46036 and 46005, followed by the nearshore buoys from north to south. The arrival of these waves at buoys 46041 and 46029 coincides with the increase of the infragravity signal on KEBB. The fact that infragravity waves at KEBB are observed when the short-period ocean waves reach the coast and not when they pass directly above KEBB demonstrates that they are generated in the nearshore region and are not simply due to direct action at the passage of the storm over the station. The same can generally be observed throughout the deployment and for storms arriving from different azimuths and having different mean wave directions. This agrees with previous observations at MOBB [*Dolenc et al.*, 2005]. Figure 3c presents more detailed spectrograms for the arrival of the short-period ocean waves to the nearshore buoys on day 2004.048. To increase the time resolution, the PSD for the vertical KEBB channel shown in the top panel is calculated from the 15-min time windows with no overlap. The time resolution of the SWD plots (bottom panels) cannot be improved since the SWD values are computed from 20-min time intervals once every hour and the raw acceleration measurements are not transmitted to the shore. The arrival of the short-period ocean waves to buoys 46041 and 46029 at 0500 UTC on day 2004.048 does not result in strong infragravity signal at KEBB yet (dashed line in Figure 3c). Instead, a slight increase of the infragravity wave energy between 70 and 100 s is observed. This signal could be due to a gradual onset of the incoming wave energy. It is also possible that this signal corresponds to infragravity energy that was transferred to seismic waves in the nearshore region and propagated to KEBB through the solid earth. A much stronger infragravity signal at KEBB is observed about 45 min later (solid line, Figure 3c). This signal is due to infragravity waves that propagated from the nearshore region to KEBB and then created pressure fluctuations at KEBB as they propagated over it. This is discussed in more detail below.
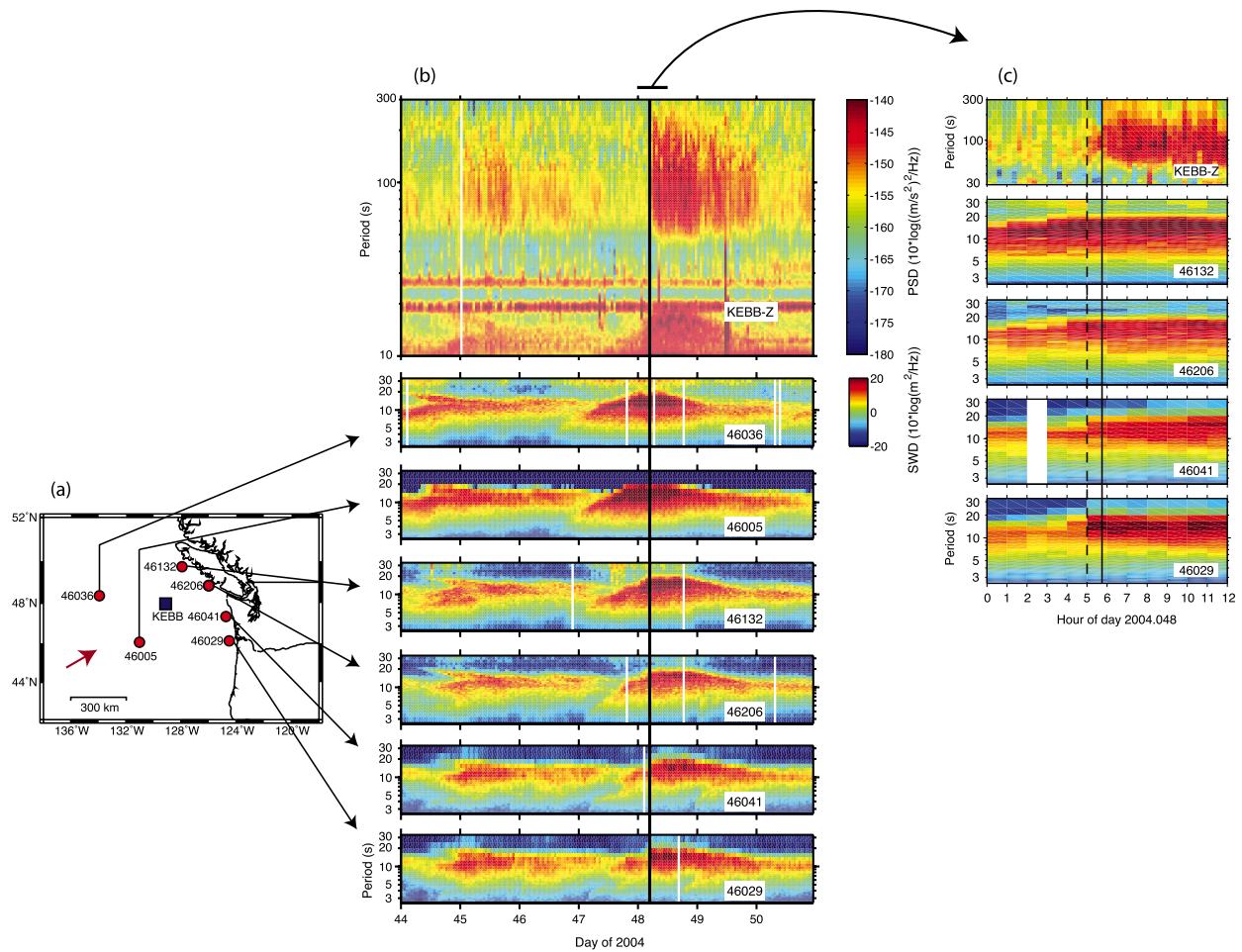
Figure 3. (a) Locations of seismic station KEBB and nearby ocean buoys. The red arrow shows the mean wave direction for the storm observed on day 2004.048. (b) Top panel: PSD for the vertical KEBB component as a function of time (13–19 February 2004) and period (10–300 s). Bottom 6 panels: The spectral wave density (SWD) of the ocean waves measured at nearby buoys. Vertical line indicates a sudden change of the infragravity peak width. It coincides with the time when the short-period ocean waves reach the coast and not when they pass directly above KEBB. (c) A closer look at the PSD for the vertical KEBB component and SWD at the nearshore buoys for the first 12 h of day 2004.048.

[13] Figure 4 shows the horizontal velocity ground motion at KEBB for the first 15 min of hours 0200, 0400, 0500, 0600, and 1100 UTC on day 2004.048. The data shown were filtered in the period band from 40 to 200 s. The results show that the horizontal motions are strongly polarized in the NW–SE direction. The polarization can be observed already for hours 0200 and 0400 UTC, before the short-period ocean waves reached the buoys 46041 and 46029. Once the stronger infragravity signal is observed at KEBB (after 0600 UTC) the motions are polarized even more strongly. Assuming that the infragravity waves observed at KEBB were generated in the nearshore region and propagated to KEBB as freely propagating gravity waves, we can approximate them as plane
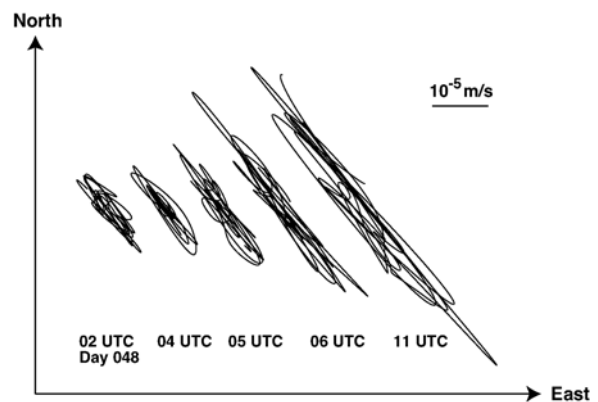

Figure 4. Horizontal velocity ground motion at KEBB for the first 15 min of hours 0200, 0400, 0500, 0600, and 1100 UTC on day 2004.048. Plotted is particle motion in the period band from 40 to 200 s.
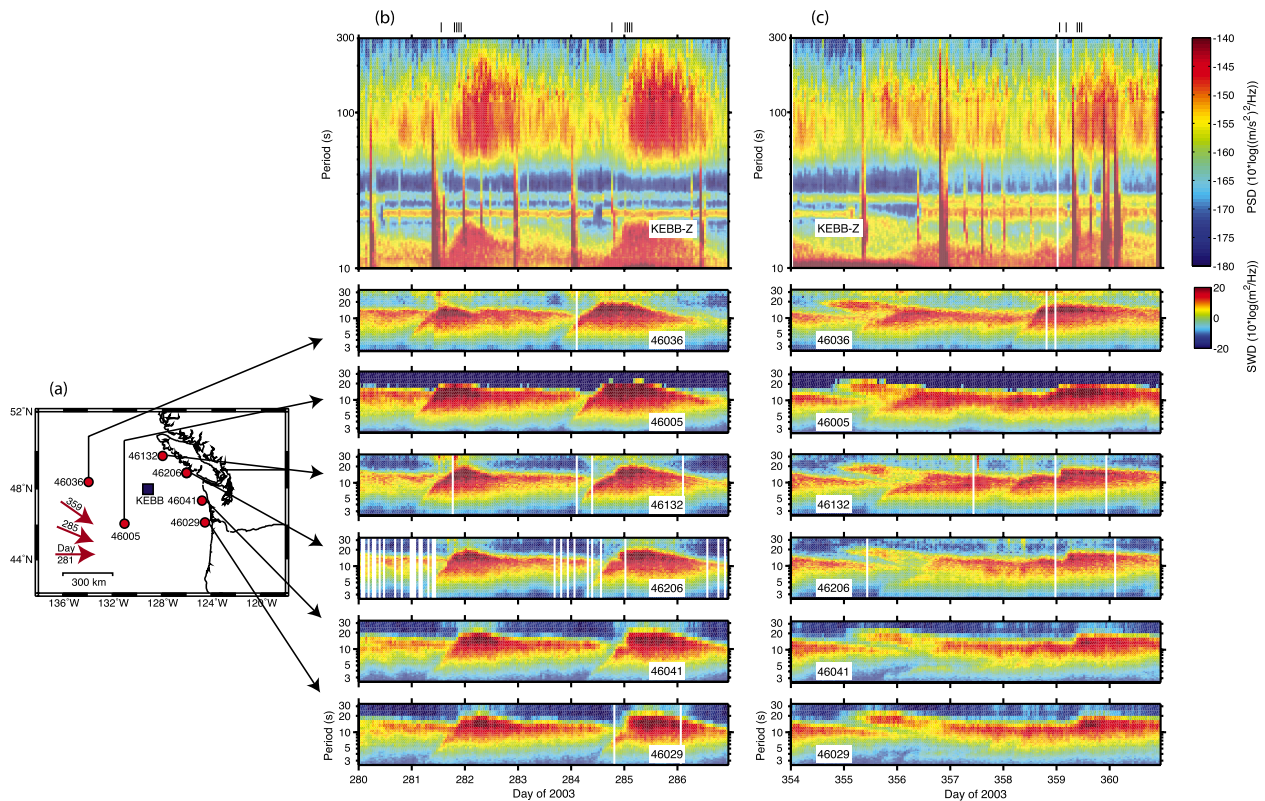
Figure 5. (a) Locations of seismic station KEBB and nearby ocean buoys. The red arrows show the mean wave directions for the storms observed on days 2003.281, 2003.284–285, and 2003.359. (b) Top panel: PSD for the vertical KEBB component as a function of time (7–13 October 2003) and period (10–300 s). Bottom 6 panels: The SWD of the ocean waves measured at nearby buoys. (c) Same as Figure 5b, only for another time period (20–26 December 2003). The lines at the top of Figures 5b and 5c indicate the hours for which the horizontal velocity ground motions are shown in Figure 6.

waves. In this case we expect the horizontal motions at the ocean bottom at KEBB to be primarily in the direction of the infragravity wave propagation. Observations at KEBB therefore suggest that the infragravity waves arrived from the SE direction, which corresponds to the nearshore region between buoys 46029 and 46050 (Figure 1). Figure 3c also shows that early on day 2004.048, strong short-period ocean waves already reached the nearshore region close to Vancouver Island, but not yet the nearshore buoys along the Washington shoreline. The fact that the horizontal motions observed early on day 2004.048 are polarized in the NW–SE direction suggests that if the infragravity waves are generated along the Vancouver Island shoreline at all, they are extremely weak.

[14] Figures 5 and 6 show examples of three additional storms with different mean wave directions as measured at buoy 46041 that produced similar results as discussed above. The 7-d time period (7–13 October 2003) shown in Figure 5b

includes a storm on day 2003.281 that included waves arriving from the W direction, and a storm on day 2003.284–285 that had waves arriving from the WNW direction. The 7-d time period (20–26 December 2003) shown in Figure 5c includes a storm that reached the coast on day 2003.359 and had the waves arriving from the NW direction. Although a signal from an earthquake (Mw6.5 Panama/Costa Rica, 0711 UTC) coincides with the time when the PSD increases at KEBB on day 2003.359, this is the best example of a storm with the mean wave direction from the NW. The three additional storms confirm that, first, the infragravity waves are observed at KEBB when the short-period ocean waves reach the coast and not when they pass directly above KEBB, and second, that the particle motion for long-period noise at KEBB is consistently polarized in the NW–SE direction (Figure 6). These, as well as other observations throughout the deployment, confirm that regardless of the incoming storm
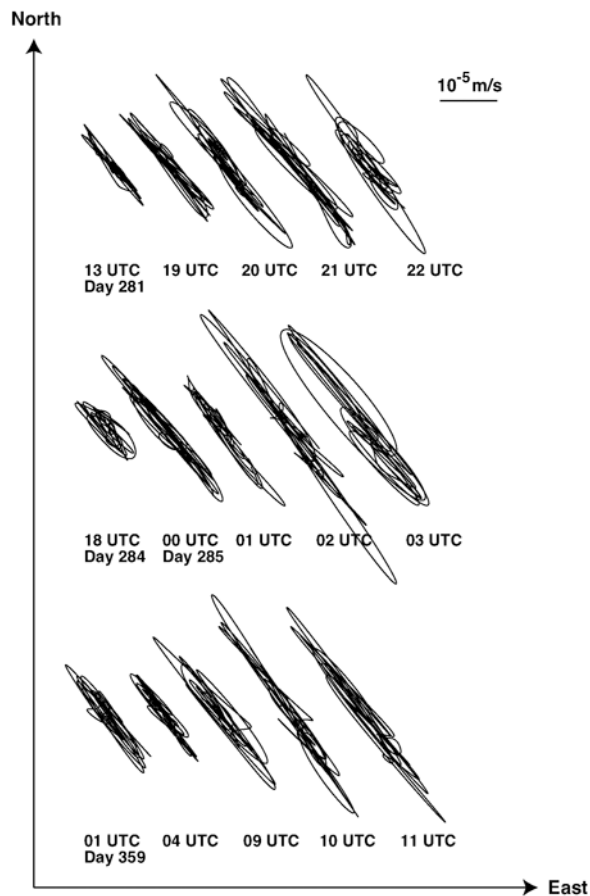
Figure 6. Horizontal velocity ground motion at KEBB for the first 15 min of hours indicated at the top of Figures 5b and 5c.

direction or the mean wave direction, the infragravity waves observed at KEBB are generated in the nearshore region SE of KEBB.

5. Modulation of Infragravity Signal

5.1. Short-Period (14–16 s) Ocean Wave Energy Modulation of the Infragravity Signal

[15] The PSD for the vertical KEBB component for a 10-d period (11–21 October 2003) is shown in Figure 7a. As before, the strongest infragravity signal (days 2003.285, 289–293) coincides with the increased energy of 5–20 s ocean waves as recorded at the local buoy 46041 (Figure 7e). Figure 7 also shows that the width of the infragravity peak changes significantly within the 10-d period. This low-frequency modulation of the infragravity signal is best seen as the variation of the period on the long-period side of the infragrav-

ity peak at which the infragravity peak rises above the noise from other sources. Figure 7b shows the envelope of the observed infragravity peak on the long-period side as defined by the PSD value of −157 dB. The infragravity peak extends to the longest periods during day 2003.285. We compare this to the significant wave height (SWH) measured at the local buoy 46041 (Figure 7c). SWH is the average of the highest 1/3 of all of the wave heights during the 20-min sampling period, calculated once every hour. Previous analysis at MOBB showed that the energy of the infragravity waves is better correlated to the wave energy in individual period bins than to the SWH, in particular when it is the shorter-period ocean waves (10 s and shorter) that contribute most to the SWH [see *Dolenc et al.*, 2005, Figure 5]. We therefore also looked at the correlation between the period of the infragravity peak envelope and the wave energy in individual frequency bins as observed at buoy 46041. Correlations between the period of the infragravity peak envelope and SWD of the ocean waves at three periods (12.5 s, 14.3 s, and 16.6 s) as well as SWH are shown in Figure 8. The best correlation was observed with 14.3 s period ocean waves for which the SWD is shown in Figures 7d and 8b. The correlation coefficient between the period of the infragravity peak envelope and the SWD observed in the individual bins at buoy 46041, as a function of the SWD bin period, is presented in Figure 8d, and confirms that the infragravity peak long-period modulation correlates the strongest with the ocean wave energy at 14–16 s. In the above analysis we used the envelope of the long-period side of the infragravity peak as an estimate of the overall infragravity energy. As the infragravity "hump" gets bigger, it also grows wider and its width is related to the overall energy of the infragravity waves. Similar results were obtained if instead of the envelope we used a total energy of the infragravity waves in the complete infragravity wave band.

5.2. Tidal Modulation of the Infragravity Signal

[16] Figure 9 compares the PSD for the vertical KEBB component to the theoretical ocean tide at buoy 46041 and to the SWD at buoy 46041 for a 7-d period (20–26 February 2004). Theoretical ocean tides were computed using the program package SPOTL [*Agnew*, 1996] and the CSR 3.0 global ocean tide model [*Eanes and Bettadpur*, 1995]. The integrated power shown in the second panel was obtained by integrating the PSD shown
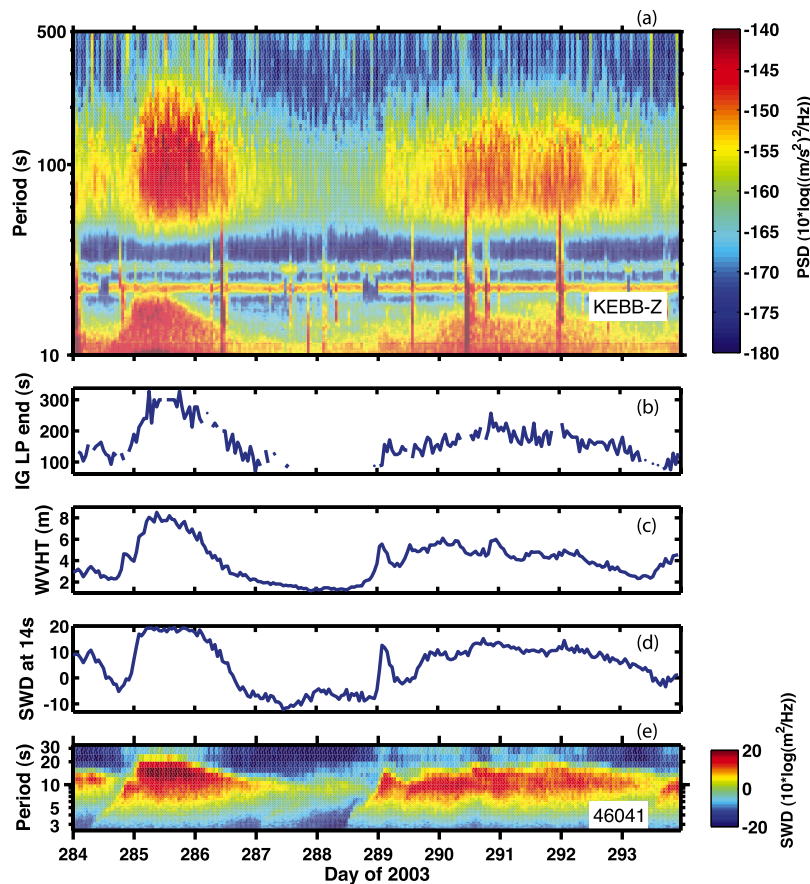
Figure 7. (a) PSD for the vertical KEBB channel as a function of time (11–20 October 2003) and period (10–500 s). (b) The envelope of the infragravity peak shown in Figure 7a, taken at the long-period end, at the threshold PSD value of −157 dB. (c) The significant wave height (SWH) at buoy 46041. (d) SWD in the 14.3 s period bin at buoy 46041. (e) SWD at buoy 46041.

in panel 3 over the infragravity wave band, from 45 s to 300 s. The top three panels show that the infragravity band is modulated in-phase with tides. The modulation is best observed when the infragravity signal is strong and the tide amplitude is large (e.g., days 2004.052−054).

[17] The modulation with a period equal to the semidiurnal tide can be seen at the short-period end of the infragravity peak (45−55 s periods) as well as throughout the entire infragravity band. Comparison of the PSD and the tides shows that the infragravity waves have less energy at low tides. This can best be seen for the strongest minima in tides that occur a few hours after the beginning of each day for this time period. Observations at KEBB agree with previous reports of tidally modulated infragravity motions on the inner-shelf at several central California sites [*Okihiro and Guza*, 1995] as well as at the ocean-bottom broadband seismic station MOBB [*Dolenc et al.*, 2005].

[18] A recent study by *Thomson et al.* [2006] suggested that tidal modulation of infragravity waves results from the energy loss that occurs in the surf zone and is due to nonlinear transfer of energy from infragravity waves to higher-frequency motions. Since the energy loss is greater when the waves propagate over the convex low-tide beach profile than over the concave high-tide profile, the observed infragravity waves have less energy at low tides [*Thomson et al.*, 2006]. A study by *Henderson et al.* [2006] showed that nonlinear energy transfers between infragravity and higher-frequency motions are responsible for most of the generation and loss of the infragravity wave energy, although in this case the tidal modulation of the infragravity waves was not observed.

[19] Since the tidal modulation of the infragravity signal occurs in the nearshore region, we can use it to identify the origin of the infragravity waves observed at KEBB. There are two parameters that we use in the analysis. First, the tidal phase
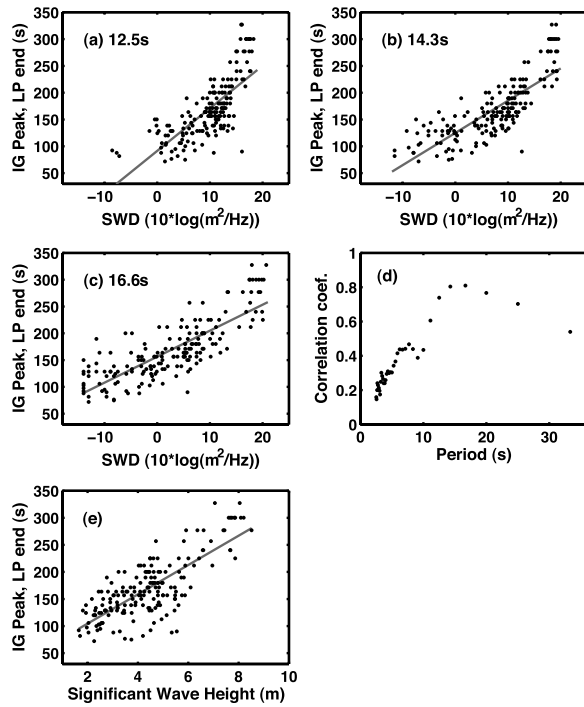
Figure 8. (a–c) Period of the infragravity peak envelope, taken at the long-period end, at the PSD value of −157 dB, as a function of the SWD observed at buoy 46041 for the 3 period bins. (d) Correlation coefficient between the period of the infragravity peak envelope and SWD observed in individual bins at buoy 46041, as a function of the SWD bin period. (e) Period of the infragravity peak envelope as a function of the SWH observed at buoy 46041. Gray lines show best linear fits to the data. The long-period modulation of the infragravity peak correlates strongest with the energy of the 14−16 s ocean waves.

changes along the shore. Figure 10 shows the differences in tidal phase at the 4 nearshore buoy locations on day 2004.053. The tide at the southernmost buoy 46050 precedes the tide at 46029 by 10 min, the tide at 46041 by 17 min, and the tide at the northernmost buoy 46206 by 29 min. Since in this region the lines of constant tidal phase extend from the coast out into the ocean [*Myers and Baptista*, 2001], we can use the same tidal phases as computed at the buoy locations for the location closer to the shore. Second, the distance to KEBB changes as we move along the shore. Since the freely traveling surface gravity waves are dispersed, we expect the difference between the arrival time of the longer- and shorter-period infragravity waves at KEBB to be a function of the distance that infragravity waves have to travel from the nearshore region to KEBB.

[20] We first calculated the PSD for the vertical KEBB channel for 15 min long time windows with no overlap. Figure 11a compares the obtained PSD in the 60 s period bin to the theoretical tide at 46041, and Figure 11b shows the PSD after it has been smoothed using a 5-point moving average. The result shows that the tidal modulation of the PSD signal is lagging behind the tidal amplitude at station 46041. We further used cross-correlation between the PSD and the tidal amplitude to determine the time advance by which the PSD needs to be shifted in order to be in phase with the local tides. For the 60 s period infragravity waves the calculated time advance is 137 min (Figure 11c), for the 90 s period waves it is 102 min, and for 112.5 s period waves it is 96 min. The correlation coefficient between the PSD in three period bins and the tides at buoy 46041 as a function of the time advance is shown in Figures 11d, 11e, and 11f. If the infragravity signal observed at KEBB were modulated in the nearshore region just east of the buoy 46041, the obtained time advance should correspond to the traveltime from the nearshore region to KEBB. Since the freely traveling surface gravity waves are dispersed, we expect the longer-period infragravity waves to arrive at KEBB first. We did the above described analysis for period bins between 50 and 128.6 s; a period range that corresponds to the strong PSD signal present within the 7-d period. We also repeated the analysis using the tides computed at the other 3 nearshore buoys. The results are shown in Figure 12 (red crosses).

[21] To compute the expected traveltimes from different nearshore regions to KEBB, we approximate the travel path of the infragravity waves by two segments; a 50 km long path above the continental shelf with an average water depth of 100 m, and the path from each buoy to the KEBB in 2000 m water depth. We used the dispersion relation for the freely traveling surface gravity waves [*Apel*, 1987]

$$\omega^2 = gk\tanh(kH) \tag{1}$$

to first solve for the wave number k. In the above equation ω is the angular frequency of the ocean gravity wave, H is the water depth, and g is gravitational acceleration. We then calculated group velocity using

$$u_g = \frac{\partial\omega}{\partial k} = \frac{g\left(\tanh(kH) + \frac{kH}{\cosh^2(kH)}\right)}{\sqrt{4gk\tanh(kH)}} \tag{2}$$
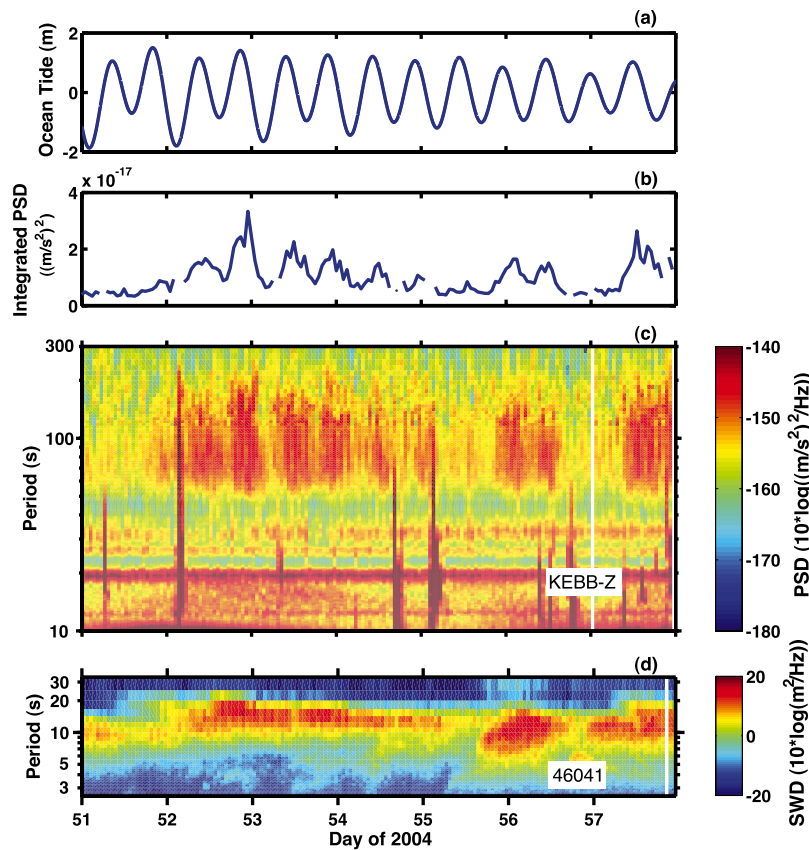
Figure 9. (a) Theoretical ocean tide at buoy 46041 for a 7-d period (20–26 February 2004). (b) The integrated power in the infragravity wave band (from 45 s to 300 s). (c) PSD for the vertical KEBB component. (d) SWD at the buoy 46041. Figures 9a and 9b show that the infragravity band is modulated in phase with tides. The modulation is best observed when the infragravity signal is strong and the tides amplitude is large (e.g., days 2004.052–054).

We used the exact form of the above equation to calculate the group velocity and not its deepwater approximation ($u_g = \frac{1}{2}\sqrt{\frac{g}{k}}$) that can be used only when ($kH \gg 1$). The computed traveltimes from the four nearshore regions to KEBB are shown in Figure 12 as blue lines. The agreement between the observed time advances (red) and expected traveltimes (blue) was estimated by computing RMS difference values that are listed in Figure 12. The results suggest that the infragravity waves that are observed at KEBB as modulated by tides originate from the nearshore region east of buoy 46041, and not from the nearshore regions farther to the north that are closer to KEBB. This is compatible with the polarization measurements reported in Figures 4 and 6.

6. Discussion

[22] Observations of the long-period seismic noise at KEBB suggest that the infragravity waves are mainly generated when the short-period ocean

waves reach the coast. The comparison of the observed dispersion of the infragravity waves at KEBB to the calculated traveltimes for different source regions further showed that the infragravity waves observed at KEBB originate from the near-shore region east of buoy 46041 and not from the nearshore regions farther to the north that are closer to KEBB. The strong polarization of the horizontal
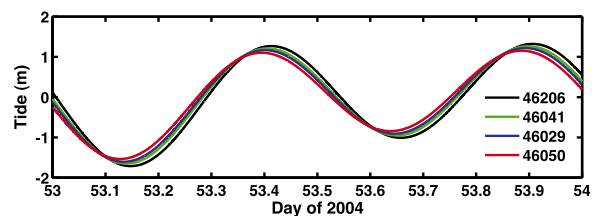

Figure 10. Theoretical ocean tide at the nearshore buoys on day 2004.053. The tide at the southernmost buoy 46050 precedes the tide at 46029 by 10 min, the tide at 46041 by 17 min, and the tide at the northernmost buoy 46206 by 29 min.
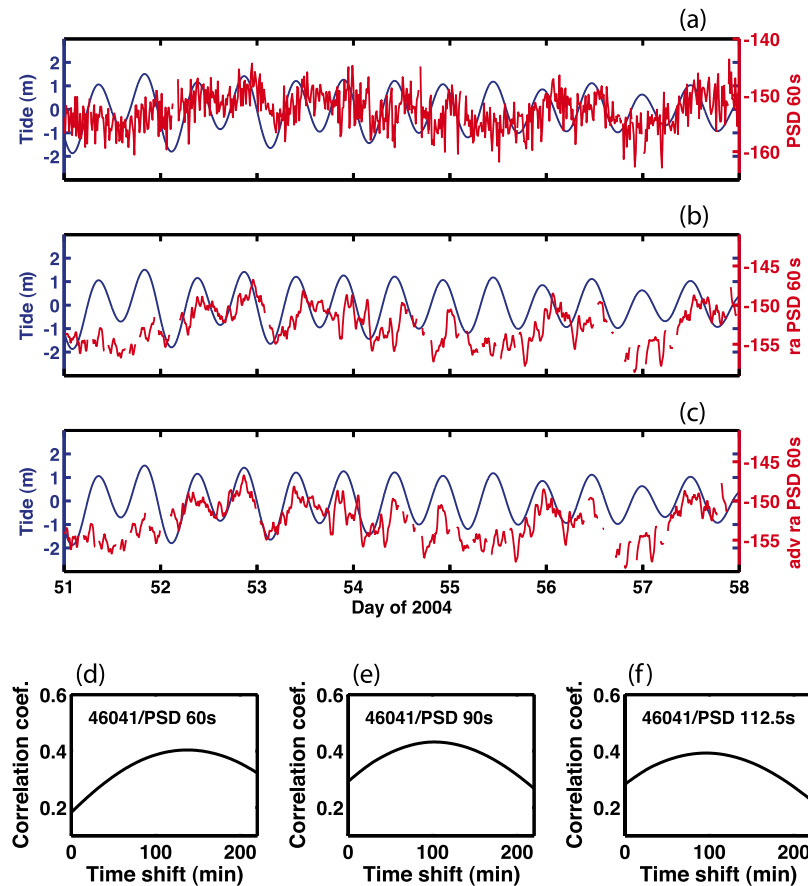
Figure 11. (a) Theoretical ocean tide at buoy 46041 (blue) and PSD in the 60 s bin for the vertical KEBB component (red) for the 7-d period. PSD was computed from 15 min long time windows with no overlap. (b) Same as Figure 11a, only that PSD curve has been smoothed using a 5-point moving average. (c) Same as Figure 11b, only that PSD (red) has been advanced 137 min to obtain the best correlation with tides (blue). (d) The correlation coefficient between the PSD in the 60 s bin for the vertical KEBB component and the theoretical ocean tide at buoy 46041, shown as a function of advance of the PSD in time. The time shift that produced the best correlation is shown in Figure 11c. (e and f) Same as Figure 11d, only that results for PSD in the 90 s and 112.5 s bin are shown.

motions at KEBB confirmed that regardless of the incoming storm direction the infragravity waves arrived to KEBB from the SE direction. The buoy 46041 is located offshore town of Taholah, Washington (47.35N, 124.29W). The difference between the coast to the north and to the south of this latitude is that the northern Washington as well as Vancouver Island coast is primarily rocky and rugged, often consisting of a wave-cut cliff. The southern Washington coast, on the other hand, is more or less a continuous, long, and wide sandy beach. The fact that the infragravity waves observed at KEBB originate from the southern Washington region might suggest that long sandy beaches play an important role in infragravity wave generation. Our results agree with a previous study by *Herbers et al.* [1995b] that observed about an order of magnitude higher infragravity wave energy

levels offshore of a sandy beach than offshore of a rocky beach for similar incident swell conditions.

[23] The entire infragravity band signal observed at KEBB is modulated in phase with tides. This can be explained by a mechanism proposed by *Thomson et al.* [2006] which suggests that the change of the beach profile from convex to concave as the tides change from low to high results in variations of the nonlinear energy transfers between infragravity and higher-frequency motions. Similar tidal modulation of the infragravity wave energy has previously been observed at MOBB [*Dolenc et al.*, 2005] and should be expected at other nearshore locations as well, since tidal changes in beach profiles are commonly observed worldwide [*Woodroffe*, 2002].
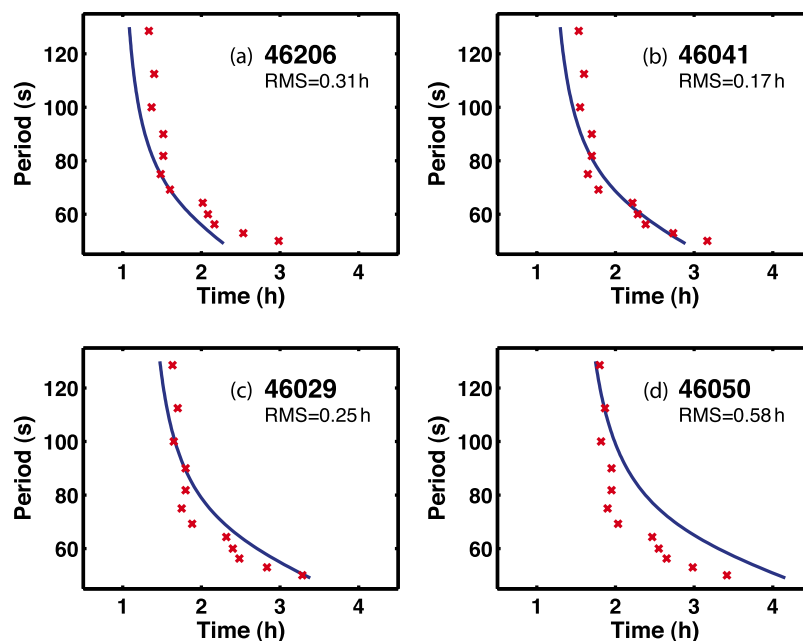
Figure 12. (a) Traveltime for the infragravity waves from the nearshore region close to buoy 46206 to KEBB computed using equation (2) (blue). The red crosses show the time advance of the PSD for individual period bin that produced the best correlation between the PSD in that period bin and the theoretical tide at buoy 46206. (b-d) Same as Figure 12a, except that locations of the other three nearshore buoys were used to compute the infragravity wave traveltimes and theoretical tides at these buoys, and used in the correlation analysis.

[24] A longer-period modulation of the infragravity signal at KEBB is also observed and is best correlated with the energy of the 14–16 s period ocean waves. This agrees with results from the MOBB deployment [*Dolenc et al.*, 2005] which showed that the modulation of the 12–14 s period ocean wave energy can be observed in the infragravity signal. This indicates that the short-period ocean waves are essential for the generation of the infragravity waves. Since the same period ocean waves are also the source of the microseisms noise observed at the double frequency, at 6–7 s, this suggests that the generation mechanisms of infragravity waves and double frequency microseisms might be closely related, as already suggested by *Rhie and Romanowicz* [2006] on the basis of a comparison of seismic noise in the microseismic and "hum" frequency bands. The generation of the double-frequency microseisms by the nonlinear interaction of ~14 s ocean waves is well documented [e.g., *Longuet-Higgins*, 1950].

[25] The observations at KEBB suggest that the infragravity waves are not generated uniformly along the shore. To minimize the long-period noise at ocean-bottom seismic stations, it is important that, prior to any nearshore deployments, we iden-

tify the regions that are least likely to generate infragravity waves. The best locations for ocean-bottom broadband stations would be in the regions with a weak average incoming short-period wave-field and/or close to a beach with a convex profile that does not change with tides. Also important is radiation of infragravity waves from adjacent beaches, refraction over smooth slopes in bathymetry, as well as reflection and refraction from submarine canyons [*Thomson et al.*, 2005, 2007]. Modeling of the spatial variability of infragravity waves should be used prior to the selection of sites for ocean-bottom stations, in particular when the target site is on the shelf and in a region with complex bathymetry.

[26] Comparison of the data observed on the horizontal KXBB channels to the ocean-bottom current data observed at ER, close to station KEBB, suggests that ocean-bottom currents dominate the long-period noise at KXBB (see Appendix A). If ocean-current measurements collocated with the KXBB seismometer existed, they could be used to confirm this. Although the collocated current measurements can help with the identification of the long-period seismic noise, the current induced tilt noise is mainly caused by seafloor currents

flowing past the instrument and by eddies spun off the back of the instrument [*Webb*, 1988; *Duennebier and Sutton*, 1995]. Since both result from turbulence, the current measurements cannot be further used to remove the current-driven tilt noise. On the other hand, the collocated pressure measurements can be directly used to remove noise due to infragravity waves [*Crawford and Webb*, 2000; *Dolenc et al.*, 2007]; therefore it is even more important to have a pressure sensor collocated with every ocean-bottom seismometer.

[27] A previous study by *Rhie and Romanowicz* [2006] identified the nearshore sources as contributing significantly to the forcing of the Earth's seismic normal modes. Results from this study seem to suggest that part of the infragravity signal is transferred to seismic waves in the nearshore region and propagates to KEBB through the solid earth. However, the insufficient time resolution of the SWD measurements at the buoys as well as the gradual onset of the storm energy for most of the storms during the deployment prevented further analysis.

7. Conclusions

[28] Observations of infragravity waves at the ocean-bottom seismic station KEBB show that the infragravity waves are generated when the short-period ocean waves reach the coast, and not when the storm passes directly above the station. This agrees with previous observations at the Monterey Bay ocean-bottom broadband station MOBB [*Dolenc et al.*, 2005]. The main difference is that MOBB was located only 40 km offshore while KEBB was located 247 km offshore Vancouver Island and 328 km offshore Washington. The additional offshore distance for KEBB enabled us to observe the dispersion of the infragravity waves and use the phase of the tidal modulation to determine their origin. The results show that infragravity waves observed at KEBB are tidally modulated, and originate from the nearshore region east of buoy 46041 and not from the nearshore regions farther to the north that are closer to KEBB. Strong polarization of the KEBB horizontal motions in the NW−SE direction also suggests that the infragravity waves arrive at KEBB from the SE direction. Another, longer-period modulation of the infragravity signal is also observed and is best correlated with the energy of the 14−16 s period ocean waves.

[29] Since the infragravity waves are not generated uniformly along the shore, modeling of their spatial variability could be used to select the best locations for future ocean-bottom seismic deployments. The observations of ever present long-period seismic noise at stations KEBB and KXBB are another reminder that noise due to infragravity waves and ocean-bottom currents is unavoidable in shallow buried ocean-bottom seismic installations and that collocated ocean current and pressure observations are needed to identify and remove the long-period noise from seismic data.

Appendix A: Observations at Station KXBB

[30] The results presented so far were obtained using the KEBB data from the first-year deployment, as the second-year KEBB as well as the KXBB data both showed increased background as well as instrumental noise. The second-year KEBB and KXBB data also included numerous data gaps that most probably resulted from lost data blocks due to insufficient data transfer rate [*Barclay*, 2005]. The average number of gaps at KEBB during the second deployment was 14/d, and 120/d at KXBB. We removed the 5 s gaps (KEBB) and 10 s gaps (KXBB) using an algorithm that employs discrete Fourier transform to interpolate gapped data [*Liepinsh*, 1996; *Sacchi et al.*, 1998]. The method provides a better estimate of missing data than a simple interpolation over the gap and allows us to compare the PSD at KEBB and KXBB to the SWD observed at the local buoys throughout the deployment. We tested the algorithm on segments that had complete data by first creating artificial gaps and then using the algorithm to estimate the missing data. The PSD plots obtained from the interpolated data were indistinguishable from the results obtained with the original data when computed with the temporal resolution used for the analysis in this paper.

[31] Figure A1 shows an example of the PSD spectrogram for the vertical and horizontal (E−W) channel at KEBB and KXBB during a 5-d period (7−11 March 2005) within the second year of the KEBB and the first year of the KXBB deployment. The gaps visible in the PSD correspond to data gaps in the time series that are longer than 5 s (KEBB) and 10 s (KXBB) and were not interpolated. Note that the color scale used for the KEBB Z component (Figure A1a) goes from −155 to −130 dB; in previous figures from the first-year KEBB deployment (e.g., Figures 3, 5−7, and 9) the color scale ranged from −180 to −140 dB. The 3 horizontal lines below 30 s that are seen throughout the 5 d
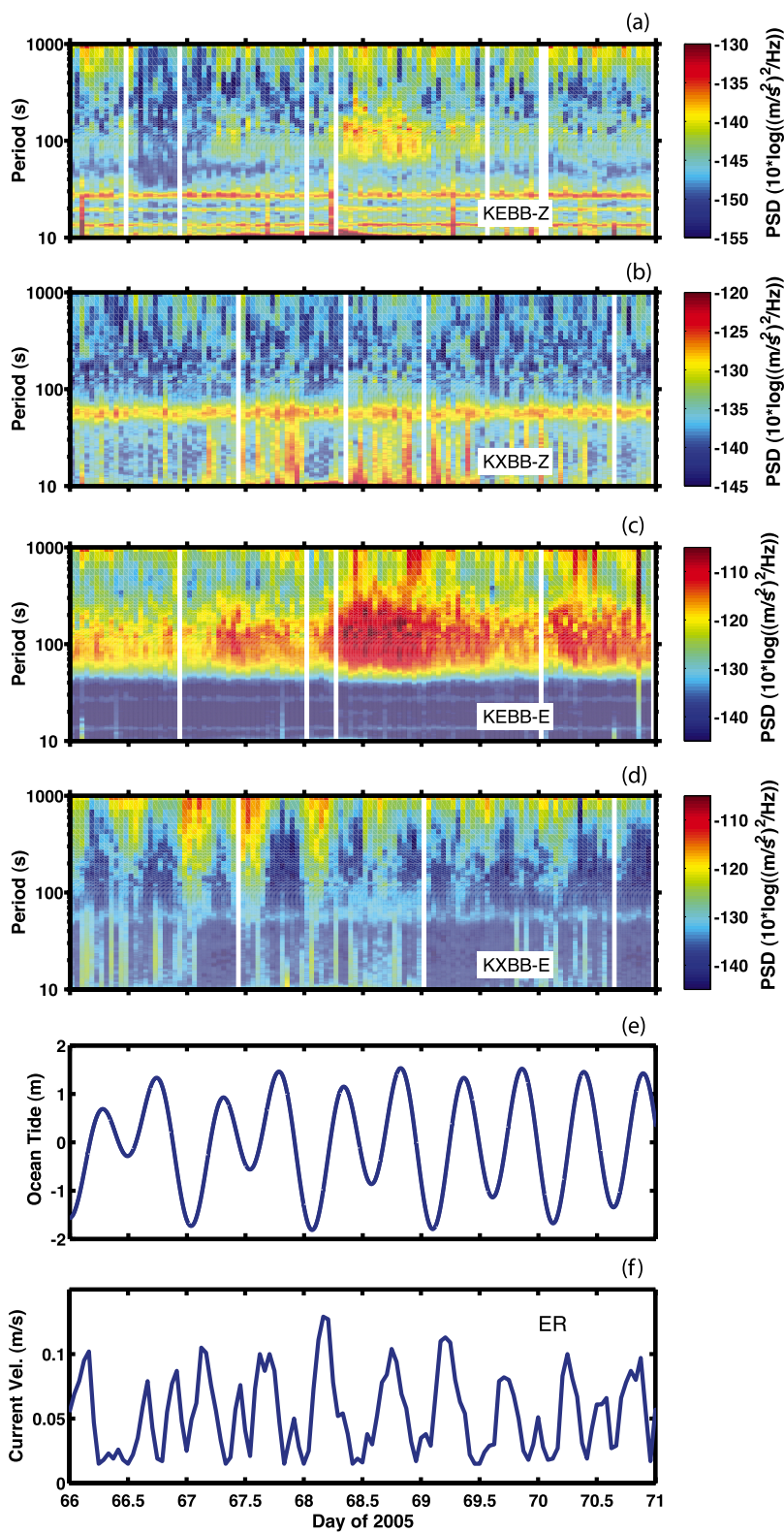
Figure A1. (a and c) PSD for the vertical and horizontal KEBB channels for a 5-d period (7–11 March 2005) during the second-year deployment. (b and d) PSD for the vertical and horizontal KXBB channels for the same time interval. (e) Theoretical tides at KXBB. (f) Near bottom ocean current velocity measured at 2103 m water depth at the Endeavour Ridge (data courtesy of R. Thomson and R. McDuff, 2005).

are probably due to instrumental noise. The infragravity signal as well as its tidal modulation can still be well observed between 50 and 200 s. Results obtained for the same time period at station KXBB are shown in the panel below (Figure A1b). In this case the color scale covers the interval from −145 to −120 dB to accommodate the strong signal around 60 s that is present on the vertical KXBB component throughout the deployment. This signal is most probably due to instrumental noise, and unfortunately completely obscures the infragravity signal on the vertical channel. The PSD for a horizontal KEBB channels is shown in Figure A1c and for a horizontal KXBB channels in Figure A1d. The same color scale is used for both panels. The results show that the infragravity signal is strong on the horizontal KEBB components where it can be observed all the way to 500 s period. The horizontal KXBB channels, on the other hand, show increased noise at periods longer than 200 s with a strong semidiurnal periodicity. Previous observations at MOBB showed that long-period noise observed on the horizontal channels is often controlled by ocean-bottom currents [*Dolenc and Romanowicz*, 2004]. At MOBB a current meter is collocated with the seismometers and the analysis of the current velocity and direction showed that ocean-bottom currents at MOBB are driven by tides [*Romanowicz et al.*, 2006]. Unfortunately station KXBB did not have a collocated ocean-bottom current meter. We first compared the PSD observed on the horizontal KXBB channels to the ocean current observations from the closest available nearshore current meters (E1 and A1 in Figure 1). In both cases the current signal was measured in shallow water and not at the ocean bottom, and showed a strong diurnal periodicity. The noise observed at the KXBB horizontals, on the other hand, shows semidiurnal periodicity. The closest location where the current data were measured at the ocean bottom was at the Endeavour Ridge, 2.7 km E of KEBB (ER in Figure 1). The theoretical ocean tides at KXBB and ocean-bottom current velocity measured at the ER are shown in Figure A1e and A1f. The comparison of the two panels shows that the ocean-bottom currents show a strong semidiurnal signature and are strongest in the hours following the lowest tides. Although the ocean-bottom currents are not available at the KXBB location, comparison of the PSD at KXBB with the current observations at ER suggests that the noise observed at KXBB horizontals is due to ocean-bottom currents.

[32] Previous analysis of the relationship between the ocean current and noise observed at the ocean bottom pressure sensor by *Webb* [1988] revealed that the seafloor pressure spectrum varies as the current to the fourth power. Using the ER current data as well as the KEBB and KXBB seismic data we tested if the same type of relationship could be observed between the current data and the seismic noise. In either case we did not observe any relationship between the two. This could be due to the fact that in our case the seismometers were buried in the ground and therefore better isolated from the currents. Also, the current meter in our case was not really collocated with the seismic sensor. Instrumental noise below 30 s that was present throughout the deployments could also have prevented us from observing a relationship between the current and the noise.

[33] Despite the additional noise at KXBB, the infragravity signal can occasionally be observed on the horizontal KXBB components. Since the infragravity signal could not be observed at the vertical KXBB component due to instrumental noise, and since only a weak infragravity signal was occasionally observed at KXBB, we did not use station KXBB in any more detailed analysis.

Acknowledgments

References

Agnew, D. C. (1996), SPOTL: Some programs for ocean-tide loading, *SIO Ref. Ser. 96-8*, 35 pp., Scripps Inst. of Oceanogr, La Jolla, Calif.

Apel, J. R. (1987), *Principles of Ocean Physics*, Academic, San Diego, Calif.

Araki, E., M. Shinohara, S. Sacks, A. Linde, T. Kanazawa, H. Shiobara, H. Mikada, and K. Suyehiro (2004), Improvement

of seismic observation in the ocean by use of seafloor boreholes, *Bull. Seismol. Soc. Am.*, *94*, 678–690, doi:10.1785/0120020088.

Barclay, A. (2005), Keck seismometer performance and data report, Visions 2005 cruise, Univ. of Wash., Seattle.

Crawford, W. C., and S. C. Webb (2000), Identifying and removing tilt noise from low-frequency (<0.1 Hz) seafloor vertical seismic data, *Bull. Seismol. Soc. Am.*, *90*, 952–963, doi:10.1785/0119990121.

Crawford, W. C., S. C. Webb, and J. A. Hildebrand (1991), Seafloor compliance observed by long-period pressure and displacement measurements, *J. Geophys. Res.*, *96*, 16,151–16,160, doi:10.1029/91JB01577.

Crawford, W. C., S. C. Webb, and J. A. Hildebrand (1998), Estimating shear velocities in the oceanic crust from compliance measurements by two-dimensional finite difference modeling, *J. Geophys. Res.*, *103*, 9895–9916, doi:10.1029/97JB03532.

Dolenc, D., and B. Romanowicz (2004), Observations of infragravity waves at the Monterey ocean bottom broadband station (MOBB), *Eos Trans. AGU*, *85*(47), Fall Meet. Suppl., Abstract S11C-08.

Dolenc, D., B. Romanowicz, D. Stakes, P. McGill, and D. Neuhauser (2005), Observations of infragravity waves at the Monterey ocean bottom broadband station (MOBB), *Geochem. Geophys. Geosyst.*, *6*, Q09002, doi:10.1029/2005GC000988.

Dolenc, D., B. Romanowicz, R. Uhrhammer, P. McGill, D. Neuhauser, and D. Stakes (2007), Identifying and removing noise from the Monterey ocean bottom broadband seismic station (MOBB) data, *Geochem. Geophys. Geosyst.*, *8*, Q02005, doi:10.1029/2006GC001403.

Duennebier, F. K., and G. H. Sutton (1995), Fidelity of ocean bottom seismic observations, *Mar. Geophys. Res.*, *17*, 535–555, doi:10.1007/BF01204343.

Duennebier, F. K., and G. H. Sutton (2007), Why bury ocean bottom seismometers?, *Geochem. Geophys. Geosyst.*, *8*, Q02010, doi:10.1029/2006GC001428.

Eanes, R., and S. Bettadpur (1995), The CSR 3.0 global ocean tide model, *Tech. Memo. CSR-TM-95-06*, Cent. for Space Res., Univ. of Texas at Austin, Austin.

Henderson, S. M., R. T. Guza, S. Elgar, T. H. C. Herbers, and A. J. Bowen (2006), Nonlinear generation and loss of infragravity wave energy, *J. Geophys. Res.*, *111*, C12007, doi:10.1029/2006JC003539.

Herbers, T. H. C., S. Elgar, and R. T. Guza (1995a), Generation and propagation of infragravity waves, *J. Geophys. Res.*, *100*, 24,863–24,872, doi:10.1029/95JC02680.

Herbers, T. H. C., S. Elgar, and R. T. Guza (1995b), Infragravity-frequency (0.005–0.05 Hz) motions on the shelf, Part II: Free waves, *J. Phys. Oceanogr.*, *25*, 1063–1079, doi:10.1175/1520-0485(1995)025<1063:IFHMOT>2.0.CO;2.

Holman, R. A., and A. J. Bowen (1982), Bars, bumps, and holes: Models for the generation of complex beach topography, *J. Geophys. Res.*, *87*(C1), 457–468, doi:10.1029/JC087iC01p00457.

Kobayashi, N., and E. Karjadi (1996), Obliquely incident irregular waves in surf and swash zones, *J. Geophys. Res.*, *101*, 6527–6542, doi:10.1029/95JC03628.

Liepinsh, V. (1996), An algorithm for evaluation a discrete Fourier transform for incomplete data, *Autom. Control Comput. Sci.*, *30*, 27–40.

Longuet-Higgins, M. S. (1950), A theory of the origin of microseisms, *Philos. Trans. R. Soc. London, Ser. A*, *243*, 1–35.

Longuet-Higgins, M., and R. Stewart (1962), Radiation stress and mass transport in gravity waves, with application to surf beats, *J. Fluid Mech.*, *13*, 481–504, doi:10.1017/S0022112062000877.

McGill, P. R., W. S. Wilcock, D. S. Stakes, A. H. Barclay, T. M. Ramirez, and D. R. Toomey (2003), A long-term seismic array on the Endeavour Segment of the Juan de Fuca Ridge, *Eos Trans. AGU*, *84*(46), Fall Meet. Suppl., Abstract B12A-0748.

McGill, P. R., D. S. Stakes, T. M. Ramirez, W. S. Wilcock, A. H. Barclay, D. R. Toomey, D. T. Durant, E. E. Hooft, T. L. Mulder, and J. P. Ristau (2004), First results from the deployment of a buried broadband seismometer on the Endeavour Segment of the Juan de Fuca Ridge, *Eos Trans. AGU*, *85*(47), Fall Meet. Suppl., Abstract T21C-0546.

Munk, W. H. (1949), Surf beats, *Eos Trans. AGU*, *30*, 849–854.

Myers, E. P., and A. M. Baptista (2001), Inversion for tides in the eastern North Pacific Ocean, *Adv. Water Resour.*, *24*(5), 505–519, doi:10.1016/S0309-1708(00)00041-5.

Okihiro, M., and R. T. Guza (1995), Infragravity energy modulation by tides, *J. Geophys. Res.*, *100*, 16,143–16,148, doi:10.1029/95JC01545.

Okihiro, M., R. T. Guza, and R. J. Seymour (1992), Bound infragravity waves, *J. Geophys. Res.*, *97*, 11,453–11,469, doi:10.1029/92JC00270.

Okihiro, M., R. T. Guza, and R. J. Seymour (1993), Excitation of seiche observed in a small harbor, *J. Geophys. Res.*, *98*(C10), 18,201–18,211, doi:10.1029/93JC01760.

Rhie, J., and B. Romanowicz (2004), Excitation of Earth's continuous free oscillations by atmosphere-ocean-seafloor coupling, *Nature*, *431*, 552–556, doi:10.1038/nature02942.

Rhie, J., and B. Romanowicz (2006), A study of the relation between ocean storms and the Earth's hum, *Geochem. Geophys. Geosyst.*, *7*, Q10004, doi:10.1029/2006GC001274.

Romanowicz, B., D. Stakes, D. Dolenc, D. Neuhauser, P. McGill, R. Uhrhammer, and T. Ramirez (2006), The Monterey Bay broadband ocean bottom seismic observatory, *Ann. Geophys.*, *49*, 607–623.

Sacchi, M. D., T. J. Ulrych, and C. J. Walker (1998), Interpolation and extrapolation using a high-resolution discrete Fourier transform, *IEEE Trans. Signal Process.*, *46*, 31–38, doi:10.1109/78.651165.

Stephen, R. A., F. N. Spiess, J. A. Collins, J. A. Hildebrand, J. A. Orcutt, K. R. Peal, F. L. Vernon, and F. B. Wooding (2003), Ocean Seismic Network Pilot Experiment, *Geochem. Geophys. Geosyst.*, *4*(10), 1092, doi:10.1029/2002GC000485.

Tanimoto, T. (2005), The oceanic excitation hypothesis for the continuous oscillations of the Earth, *Geophys. J. Int.*, *160*, 276–288, doi:10.1111/j.1365-246X.2004.02484.x.

Thomson, J., S. Elgar, and T. H. C. Herbers (2005), Reflection and tunneling of ocean waves observed at a submarine canyon, *Geophys. Res. Lett.*, *32*, L10602, doi:10.1029/2005GL022834.

Thomson, J., S. Elgar, B. Raubenheimer, T. H. C. Herbers, and R. T. Guza (2006), Tidal modulation of infragravity waves via nonlinear energy losses in the surfzone, *Geophys. Res. Lett.*, *33*, L05601, doi:10.1029/2005GL025514.

Thomson, J., S. Elgar, T. H. C. Herbers, B. Raubenheimer, and R. T. Guza (2007), Refraction and reflection of infragravity waves near submarine canyons, *J. Geophys. Res.*, *112*, C10009, doi:10.1029/2007JC004227.

Tucker, M. J. (1950), Surf beats: Sea waves of 1 to 5 min. period, *Proc. R. Soc. London, Ser. A*, *202*, 565–573.

Webb, S. C. (1988), Long-period acoustic and seismic measurements and ocean floor currents, *IEEE J. Oceanic Eng.*, *13*, 263–270, doi:10.1109/48.9239.

Webb, S. C. (1992), The equilibrium microseism spectrum, *J. Acoust. Soc. Am.*, *92*, 2141–2158, doi:10.1121/1.405226.

Webb, S. C. (1998), Broadband seismology and noise under the ocean, *Rev. Geophys.*, *36*, 105–142, doi:10.1029/97RG02287.

Webb, S. C. (2007a), The Earth's 'hum' is driven by ocean waves over the continental shelves, *Nature*, *445*, 754–756, doi:10.1038/nature05536.

Webb, S. C. (2007b), Forcing by infragravity waves interacting over the deep ocean basins is important to maintaining the Earth's seismic normal mode background (the 'Earth's hum'), *Eos Trans. AGU*, *88*(52), Fall Meet. Suppl., Abstract S11D-07.

Webb, S. C., and W. C. Crawford (1999), Long-period seafloor seismology and deformation under ocean waves, *Bull. Seismol. Soc. Am.*, *89*, 1535–1542.

Webb, S. C., X. Zhang, and W. Crawford (1991), Infragravity waves in the deep ocean, *J. Geophys. Res.*, *96*, 2723–2736, doi:10.1029/90JC02212.

Wilcock, W. S. D., P. R. McGill, E. E. Hooft, D. R. Toomey, H. M. Patel, D. S. Stakes, A. H. Barclay, T. M. Ramirez, and R. T. Weekly (2007), The deployment of a long-term seafloor seismic network on the Juan de Fuca Ridge, paper presented at the MTS/IEEE Oceans 2007 Meeting, Mar. Technol. Soc., Vancouver, 29 Sept. to 4 Oct.

Woodroffe, C. D. (2002), *Coasts: Form, Process and Evolution*, Cambridge Univ. Press, New York.